7. G. Wall, P. D. Varga-Weisz, R. Sandaltzopoulos, P. B. Becker, *EMBO J.* **14**, 1727 (1995).
8. J. A. Armstrong and B. M. Emerson, *Mol. Cell. Biol.* **16**, 5634 (1996).
9. M. J. Pazin, R. T. Kamakaka, J. T. Kadonaga, *Science* **266**, 2007 (1994).
10. M. J. Pazin *et al.*, *Genes Dev.* **10**, 37 (1996).
11. S. Alberti, S. Oehler, B. von Wilcken-Bergmann, B. Müller-Hill, *EMBO J.* **12**, 3227 (1993); J. Chen, S. Alberti, K. S. Matthews, *J. Biol. Chem.* **269**, 12482 (1994).
12. The DNA sequence of this plasmid is available upon request. The 183-bp DNA interval was used to represent approximately one nucleosomal repeat.
13. R. T. Kamakaka, M. Bulger, J. T. Kadonaga, *Genes Dev.* **7**, 1779 (1993); M. Bulger and J. T. Kadonaga, *Methods Mol. Genet.* **5**, 241 (1994).
14. T. Tsukiyama and C. Wu, *Cell* **83**, 1011 (1995); T. Tsukiyama, C. Daniel, J. Tamkun, C. Wu, *ibid.*, p. 1021.
15. P. D. Varga-Weisz, T. A. Blank, P. B. Becker, *EMBO J.* **14**, 2209 (1995).
16. C. Wu, *Nature* **286**, 854 (1980); S. A. Nedospasov and G. P. Georgiev, *Biochem. Biophys. Res. Commun.* **92**, 532 (1980).
17. The inclusion of R3 protein, IPTG, or apyrase (or all three) did not affect the quality of the chromatin, as determined by micrococcal nuclease digestion analysis (Fig. 3) and by DNA supercoiling analysis (*26*). In this work, each experimental condition was explored at least twice but more commonly several times, to ensure reproducibility of the data.
18. M. C.-T. Hu and N. Davidson, *Cell* **48**, 555 (1987); M. Brown *et al.*, *ibid.* **49**, 603 (1987); M. Gossen, A. L. Bonin, H. Bujard, *Trends Biochem. Sci.* **18**, 471 (1993).
19. We did not observe the 10-bp repeating DNase I digestion pattern (*1*) that is generated with rotationally positioned nucleosomes. Hence, there is no evidence suggesting that the chromatin contains rotationally positioned nucleosomes.
20. C. L. Peterson and J. W. Tamkun, *Trends Biochem. Sci.* **20**, 143 (1995); R. E. Kingston, C. A. Bunker, A. N. Imbalzano, *Genes Dev.* **10**, 905 (1996); T. Krude and S. C. R. Elgin, *Curr. Biol.* **6**, 511 (1996).
21. P. Beard, *Cell* **15**, 955 (1978); C. Spadafora, P. Oudet, P. Chambon, *Eur. J. Biochem.* **100**, 225 (1979).
22. For primer extension footprinting, micrococcal nuclease is more effective than DNase I for the detection of a nucleosome footprint [see, for example, (*4*)], whereas DNase I is the preferred reagent for detecting sequence-specific DNA-bound factors, such as R3 (compare, for example, Figs. 1B and 2).
23. With other factors and in different contexts, an activation region might be required for binding to the chromatin template, especially in cases of cooperative binding of transcription factors with other proteins that is mediated through interactions with the transcriptional activation domain. In addition, we do not imply that all sequence-specific DNA binding proteins (either prokaryotic or eukaryotic) must necessarily alter chromatin structure.
24. S. N. Ho, S. R. Biggar, D. M. Spencer, S. L. Schreiber, G. R. Crabtree, *Nature* **382**, 822 (1996).
25. A. Reik, G. Schütz, A. F. Stewart, *EMBO J.* **10**, 2569 (1991); A. Schmid, K.-D. Fascher, W. Hörz, *Cell* **71**, 853 (1992); E. Verdin, P. Paras Jr., C. Van Lint, *EMBO J.* **12**, 3249 (1993).
26. P. Bhargava, M. J. Pazin, E. P. Geiduschek, J. T. Kadonaga, unpublished data.
27. We thank J. Newport, A. Wurster, J. Tyler, T. Burke, K. Robinson, M. Levenstein, L. DeVito, and A. Kutach for critical reading of the manuscript; K. Matthews (Rice University) for the generous gift of R3 protein; and M. Ouhammouch (University of California San Diego) for further purification of R3. P.B. held an Overseas Fellowship from the Department of Biotechnology, Government of India. J.T.K. is a Presidential Faculty Fellow. This work was supported by grants to J.T.K. from NSF and the Council for Tobacco Research USA, and to J.T.K and E.P.G. from the National Institute of General Medical Sciences.

12 December 1996; accepted 10 March 1997

Light-Induced Structural Changes in Photosynthetic Reaction Center: Implications for Mechanism of Electron-Proton Transfer

M. H. B. Stowell,* T. M. McPhillips,† D. C. Rees,‡ S. M. Soltis, E. Abresch, G. Feher‡

High resolution x-ray diffraction data from crystals of the *Rhodobacter sphaeroides* photosynthetic reaction center (RC) have been collected at cryogenic temperature in the dark and under illumination, and the structures were refined at 2.2 and 2.6 angstrom resolution, respectively. In the charge-separated $D^+Q_AQ_B^-$ state (where D is the primary electron donor (a bacteriochlorophyll dimer), and Q_A and Q_B are the primary and secondary quinone acceptors, respectively), Q_B^- is located approximately 5 angstroms from the Q_B position in the charge-neutral (DQ_AQ_B) state, and has undergone a 180° propeller twist around the isoprene chain. A model based on the difference between the two structures is proposed to explain the observed kinetics of electron transfer from $Q_A^-Q_B$ to $Q_AQ_B^-$ and the relative binding affinities of the different ubiquinone species in the Q_B pocket. In addition, several water channels (putative proton pathways) leading from the Q_B pocket to the surface of the RC were delineated, one of which leads directly to the membrane surface.

The primary processes of photosynthesis, the conversion of electromagnetic energy (light) into chemical energy, are mediated by an integral membrane protein-pigment complex called the reaction center (RC) in which a sequence of photoinduced electron and proton-transfer reactions take place (*1*, *2*). Our knowledge of these processes was greatly enhanced through the determination of the three-dimensional structure of the RC from two purple photosynthetic bacteria: *Rhodopseudomonas viridis* (*3*, *4*) and *Rhodobacter sphaeroides* (*5*–*8*). In previous structure determinations, the primary reactants were in the neutral state, that is, no electron transfer (charge separation) had taken place. Several independent experimental findings, however, point toward a structural change accompanying charge separation (*9*–*15*). A particularly dramatic effect was observed (*11*) when the rate of electron transfer in RCs that were frozen under illumination was compared with that of those frozen in the dark. The rate of the electron transfer from the primary ubiquinone Q_A^- to the secondary ubiquinone Q_B was increased by several orders of magnitude when RCs were frozen under illumination, that is, in the charge separated state, as compared to RCs frozen in the dark.

We have now determined the structural changes accompanying charge separation in the RC and used them as a basis for a model to explain changes in the kinetics of electron transfer observed on freezing. The changes were obtained by comparing the structure of RCs in single crystals cooled to cryogenic (~90 K) temperatures under illumination (the light structure) with the structure of RCs cooled to cryogenic temperatures in the dark (the dark structure). In our experiments, we used tetragonal crystals of *Rb. sphaeroides* R-26, which had been obtained earlier by Allen (*16*). Our crystals diffracted at cryogenic temperatures to higher resolution (1.9 Å in the dark state) than previously reported RC crystals. Data collection and refinement to 2.2 Å resolution has led to the determination of the positions of a number of water molecules that provide several possible pathways for protons from the aqueous phase to the Q_B pocket. Two of these proton "channels" are delineated in detail; one of these has been reported (*8*). The importance of water molecules for proton transfer to reduced Q_B is discussed below.

RCs from *Rb. sphaeroides* R-26 were isolated and purified (*17*). Crystallization conditions were similar to those described (*16*). Crystals grew in 1 to 3 weeks to a thickness of 0.1 to 0.2 mm in space group $P4_32_12$ (unit cell dimensions $a = b = 140.1$ Å and $c = 271.6$ Å), with two RCs in the asymmetric unit (Table 1). Typical crystals

M. H. B. Stowell, T. M. McPhillips, D. C. Rees, Division of Chemistry and Chemical Engineering, 147-75CH, California Institute of Technology, Pasadena, CA 91125, USA.
S. M. Soltis, Stanford Synchrotron Radiation Laboratory, P.O. Box 4349, Bin 69, Stanford, CA 94309, USA.
E. Abresch, G. Feher, Department of Physics, 0319, University of California, San Diego, 9500 Gilman Drive, La Jolla, CA 92093–0319, USA.

*Present address: Medical Research Council, Laboratory of Molecular Biology, Cambridge CB2 2QH, UK.
†Present address: Stanford Synchrotron Radiation Laboratory, P.O. Box 4349, Bin 69, Stanford, CA 94309, USA.
‡To whom correspondence should be addressed.

showed a 60 to 70% Q_B occupancy as assayed with a microspectrophotometer (*18*). The Q_B occupancy, was increased by soaking the crystals in 1 mM ubiquinone-2 (*19*) for 2 days before data were collected. The dark-adapted crystals were plunged into liquid nitrogen and transferred via cryo-transfer tongs (*20*) to a goniostat cooled with a stream of nitrogen to ~90 K (*21*). Formation of the charge separated state $D^+Q_AQ_B^-$ (where D^+ is the primary donor, a bacteriochlorophyll dimer) was accomplished by illuminating a crystal with a filtered tungsten light source (bandpass 550 to 900 nm). The illumination conditions necessary to create $D^+Q_AQ_B^-$ were deduced from light saturation curves (*22*) in control crystals (Fig. 1). A 0.2-mm thick crystal required 0.4 W/cm^2 (150-ms pulse) to reach 90% charge separation. The crystals investigated by x-ray diffraction were illuminated for 150 ms with 0.5 W/cm^2 light directly above a liquid nitrogen bath and plunged into the bath under illumination to trap ~90% of the RCs in the charge separated state. The sample was transferred to the goniostat, and a constant illumination of 10 mW/cm^2 was maintained. Dark-adapted crystals were kept in dim light (<1 mW/cm^2) during manipulations and data collection. From the saturation curves described above, the dark crystals were >95% in the neutral state DQ_AQ_B.

The overall structure of the *Rb. sphaeroides* RC in the DQ_AQ_B state (dark structure), including the cofactors and the polypeptide folds of the three (H, M, and L) subunits, follows, with only minor differences, the structure that has been previously described (*1*, *5*–*8*). We focus, therefore, on the location of Q_B (and its surroundings) where the largest changes occur upon charge separation. The electron density map (Fig. 2A) shows the position of the ubiquinone molecule in the Q_B binding site (Q_{B1}). It is located in a pocket (Fig. 3) with the O1 of Q_B 7.2 Å from the Nδ of His^{L190}. The carbonyl oxygen O4 forms a single hydrogen bond with the amide backbone of Ile^{L224}, in a manner similar to that described (*8*). This is in contrast with room temperature FTIR (Fourier transform infrared) data which suggested that the two carbonyl oxygens form weak and equivalent hydrogen bonds (*23*). The ubiquinone ring stacks directly on the conserved Phe^{L216} in a parallel manner (Fig 3B), suggesting that this interaction contributes to the binding affinity of the ubiquinone. Further experimental support for this interaction comes from a herbicide resistant mutant of the *Rps. viridis* RC, in which Phe^{L216} is replaced with serine, resulting in an RC with reduced affinity (60 μM versus 4.5 μM for wild type) for ubiquinone (*24*). The atomic displacement factor of Q_B is greater than that of Q_A (43 Å^2 compared to 29 Å^2), an indication of a more disordered structure or a lowered occupancy at the Q_B site as compared to the Q_A site, which is fully occupied. The electron density between the bound ubiquinone and His^{L190} and Glu^{L212} is somewhat problematic. It can be modeled either by three water molecules, or by a partially occupied ubiquinone at a second binding site (Q_{B2}) or a combination of both. A partially occupied ubiquinone site is likely, and is assumed in the model discussed below.

The positions of ubiquinone in the Q_B pocket of dark adapted crystals reported by various groups differ significantly from each other (Fig. 4). There are several possible sources for this discrepancy. (i) There may be differences in the extent of dark adaptation. (ii) The position of ubiquinone in the Q_B pocket has been more difficult to establish because of the lower occupancy at the Q_B pocket and the lower resolution of previous structure determinations. (iii) Variability in sample preparations, specifically in regard to the detergent, has been shown to influence the binding of ubiquinone in the Q_B pocket (*25*). (iv) Electrons created by the x-ray irradiation during data collection may reduce ubiquinone in the Q_B pocket. At room temperature, the reduced quinone can move to the Q_{B2} position, whereas at 90 K it remains frozen in the Q_{B1}

Table 1. Data collection and refinement statistics. Data were collected at beamline 7-1 of the Stanford Synchrotron Radiation Laboratory (λ = 1.08 Å) with a 30-cm MAR Research imaging plate system. The resolution of the dark state crystal was limited to 2.2 Å by the detector setting. Data were processed with the DENZO/HKL package (*43*) and merged and scaled with Rotavata-Agrovata of the CCP4 program suite (*44*). Molecular replacement was performed with MERLOT (*45*). The molecular replacement solution without ubiquinones was used to calculate Hendrickson-Lattman coefficients (*46*) with PHASES (*47*) using Sim's weighting. These starting phase probabilities were utilized in a series of solvent flattening and twofold averaging cycles as implemented in SOLOMON (*48*). The SOLOMON electron density maps were of excellent overall quality and allowed straightforward rebuilding of the starting model with TOM/FRODO and O (*49*). Iterative cycles of model building, X-PLOR refinement (*50*), without NCS twofold restrictions and inspection of $2F_o - F_c$ and $F_o - F_c$ electron density maps lead to the present models. The final models contain two RCs, four ubiquinones, eight bacteriochlorophylls, four bacteriopheophytins, two irons, and four LDAO molecules for a total of 13929 protein atoms. The dark-adapted structure contains 468 waters and the light-adapted structure contains 60 waters. Residual electron density that has not yet been modeled in the present structures is indicative of additional detergent molecules surrounding the RCs, as well as a large number of unmodeled waters. Molecular representations were prepared with the program SETOR (*51*).

	DQ_AQ_B state (dark)	$D^+Q_AQ_B^-$ state (light)
Data collection		
Resolution range (Å)	30.0–2.2	30.0–2.6
Observations (unique)	335,463 (114,087)	203,621 (74,104)
Average I/σ (last shell)	19.5 (3.1)	14.3 (2.6)
R_{sym} (last shell) (%)	5.6 (14.6)	8.5 (16.0)
Completeness (%)	86	88
Redundancy	2.9	3.1
Refinement		
Resolution (Å)	10–2.2	10–2.6
Reflections	112,234	71,316
R_{cryst} (%)	22.0	21.5
R_{free} (%)	27.0	29.9
rms bond distance deviation (Å)	0.010	0.014
rms bond angle deviation (°)	2.60	2.89

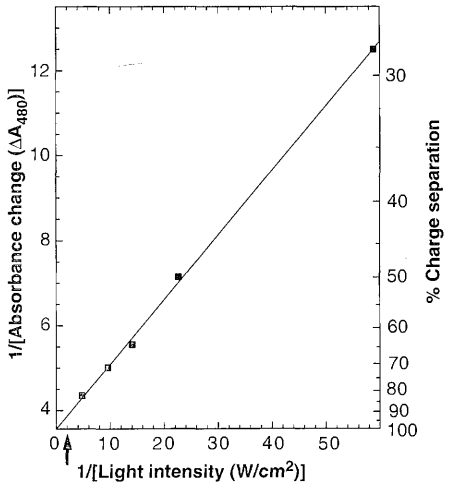

Fig. 1. Dependence of the extent of charge separation (which is proportional to the absorbance change ΔA_{480}) on light intensity in a single, 0.2-mm-thick crystal of RCs from *Rb. sphaeroides* at 295 K. The left ordinate is the reciprocal of the optical absorbance change; the intercept gives ΔA_{MAX} for 100% charge separation. The right ordinate shows the percentage charge separation. A light intensity of 0.5 W/cm^2 (see arrow) was used for the crystals investigated by x-ray diffraction, which corresponds to 92% charge separation. A tungsten projector lamp was used with band pass filters from 550 to 900 nm.

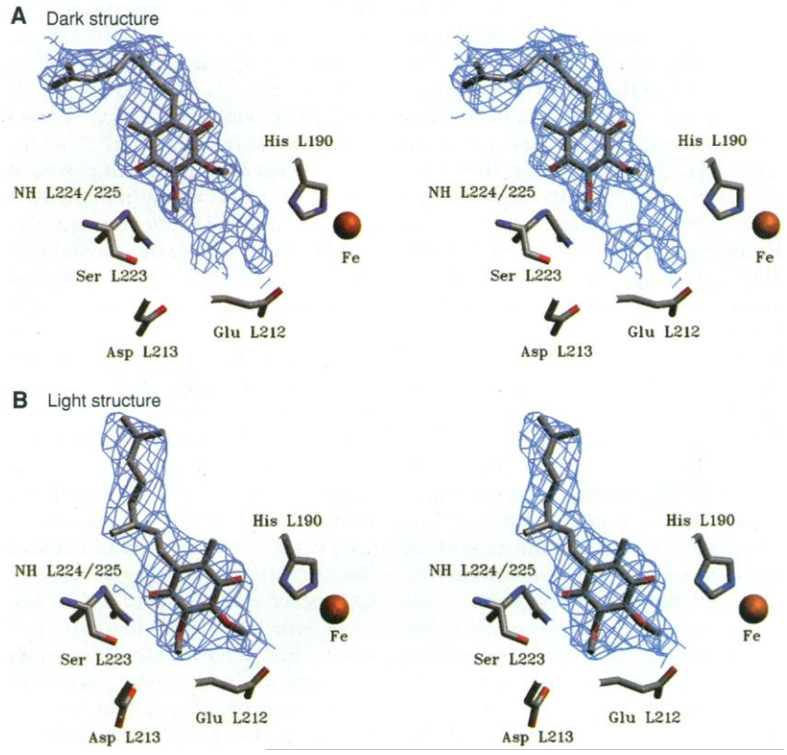

Fig. 2. (**A**) Dark structures. Stereoview of the final $2F_o - F_c$ omit, refined electron density at the Q_B binding pocket in the DQ_AQ_B (dark) state, contoured at 1σ. The ubiquinone is bound in the position referred to as the Q_{B1} site. The electron density between the Q_{B1} site and Glu^{L212} and His^{L190} is postulated to be due to partial occupancy of ubiquinone at the second site Q_{B2}. Side chain residues from the dark RC structure are indicated. (**B**) Light structures. Stereoview of the final $2F_o - F_c$ omit refined electron density at the Q_B binding pocket in the $D^+Q_AQ_B^-$ (light) state, contoured at 1σ. The ubiquinone is now in a position referred to as the Q_{B2} site, which is ~4.5 Å removed from the Q_{B1} site shown in (A). In addition, the ubiquinone has undergone a 180° propeller twist with respect to the Q_{B1} site observed in the dark structure. Side chain residues from the light RC structure are indicated. Oxygen, nitrogen, and carbon atoms are colored red, blue, and gray, respectively.

position. This could explain why the position of Q_B in several of the room temperature structures are closer to that observed in the charge separated state discussed below.

The higher resolution of this work enabled us to determine the location of water molecules. In particular, two distinct water channels, P1 and P2, that connect the Q_B pocket with the surface of the protein are shown in Fig. 5. P1 is essentially identical to the water chain reported earlier (8).

The structure of the charge separated $D^+Q_AQ_B^-$ state (light structure) is approximately the same as that of the DQ_AQ_B (dark) structure. The O4 carbonyl of the Q_B semiquinone hydrogen bonds to His^{L190} and the O1 carbonyl hydrogen bonds to the backbone amide nitrogen of Ile^{L224} (Figs. 2B and 3). This binding site is similar to the partially occupied Q_{B2} site postulated for the dark structure. The refined atomic displacement parameters for Q_B^- are similar to those of Q_A, indicative of a nearly fully occupied ubiquinone at this site. In addition to the L224 amide nitrogen, Ser^{L223} and the backbone amide of L225 are both ~3.1 Å from the O1 carbonyl of the ubiquinone and may form a second set of hydrogen bonds (albeit longer) to the ubisemiquinone anion. The presence of these three hydrogen bonds to the O1 carbonyl of the ubisemiquinone at the Q_{B2} site, especially the longer interactions with Ser^{L223} and L225 amide, are consistent with ENDOR studies on native and $Ser^{L223} \rightarrow$ Ala mutant RCs (26).

The most striking observation in the light-adapted structure is a 4.5 Å (center to center distance) movement of the ubisemiquinone toward the cytoplasm with an accompanying 180° propeller twist about the isoprene tail (Fig. 3). There are fewer well-ordered water molecules than in the DQ_AQ_B structure. Particularly striking is the observation that Glu^{H173}, located along the P2 water channel, is disordered compared to either Glu^{H173} in the dark structure or to the surrounding residues in the light structure. This suggests movement of water (protons) within the P1 and P2 channels that is concomitant with formation of the $D^+Q_AQ_B^-$ state.

A model of the electron transfer mech-

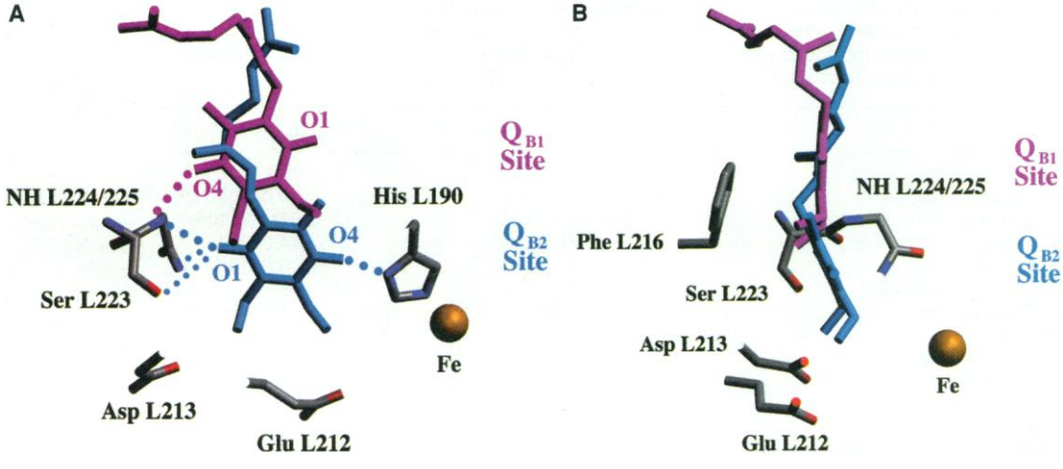

Fig. 3. Comparison of the dark (DQ_AQ_B) and the light ($D^+Q_AQ_B^-$) RC structures in the Q_B binding pocket. The dark and light RC structures are colored red and blue, respectively. Hydrogen bonds are indicated with dotted lines, where bond distances of less than and greater than 2.9 Å are indicated by large and small dots, respectively. In the light RC structure, the ubiquinone has moved ~4.5 Å and undergone a 180° propeller twist. Side chain residues from the light RC structure are indicated. Oxygen, nitrogen, and carbon atoms are colored red, blue, and gray, respectively. Orthogonal views of this region are provided in panels **A** and **B**.

anism from $Q_A^-Q_B$ to $Q_AQ_B^-$ needs to explain the observation that at low temperatures (~90°K) the electron transfer from $Q_A^-Q_B$ to $Q_AQ_B^-$ is completely blocked in RCs cooled in the dark, whereas the electron transfer proceeds readily when RCs are frozen under illumination (*11*). The differences between the light and dark structures of the RCs offer a straightforward and simple explanation of these observations. We postulate a model in which the ubiquinone can assume two positions; in one, electron transfer from Q_A^- is inhibited, in the other it is not. In the dark-adapted RCs, the position Q_{B1} (Figs. 2 and 3) is thermodynamically favored. In this position, the distance between the carbonyl oxygen O1 of Q_B and Nδ of His^{L190} is 7.2 Å. It is, therefore, disconnected from the most direct pathway for electron transfer from Q_A^- and hence, electron transfer from $Q_A^-Q_B$ to $Q_AQ_B^-$ is inhibited. However, a fraction of RCs exist in an activated state Q_{B2} corresponding to a quinone position that is ~5 Å removed from Q_{B1}. In this position, the ubiquinone is hydrogen-bonded to His^{L190} and electron transfer from Q_A^- can readily proceed. This position corresponds to the residual patch of electron density of the dark structure (Fig. 2A). We propose that the movement of the quinone from Q_{B1} to the Q_{B2} position is a necessary prerequisite for electron transfer from $Q_A^-Q_B$ to $Q_AQ_B^-$. The observed activation energy (*27*) represents the barrier between these two states. The main contribution to the activation energy is probably the breaking of the hydrogen bond from O1 to the backbone amide of Ile^{L224} (Figs. 2 and 3) and the energy associated with the 180° propeller twist. The above model is also consistent with the observation that the measured electron transfer rate from $Q_A^-Q_B$ to $Q_AQ_B^-$ is independent of the redox potential (that is, the driving force) of different ubiquinones substituted in the Q_A site, demonstrating that the rate-limiting step is not electron transfer (*28*).

In the light-adapted structure of the RC, the ubiquinone forms a hydrogen bond with His^{L190}, thereby favoring the Q_{B2} site (Figs. 2B and 3). In this position, electron transfer can readily take place, as experimentally observed. The ground state (dark) x-ray crystal structure that has been universally reported is not the kinetically active structure for electron transfer. Contributions from possible light-induced structural changes upon forming $D^+Q_A^-Q_B$ (*29*) to the electron transfer from $D^+Q_A^-Q_B$ to $D^+Q_AQ_B^-$ require further study.

After the one-electron reduction of Q_B discussed above, a second electron is transferred to Q_B^-. The doubly reduced ubiquinone is protonated to form the ubiquinol (Q_BH_2), which leaves the RC (*30*), initiating the formation of the proton gradient across the plasma membrane that drives ATP synthesis (*31*). Thus, the protonation of Q_B and the release of quinol are two fundamentally important processes. The main question associated with the protonation concerns the mechanism by which protons are transferred from the outside, aqueous phase, to the Q_B site which is buried inside the RC (*32*). The generally accepted view is that protons move along a chain of proton donor and acceptor groups. These groups could be either side chains of protonatable amino acids or water molecules. Several of the amino acids in the chain have been identified in *Rb. sphaeroides* by site-directed mutagenesis (*33–38*). The role of the water molecules has been less well estab-

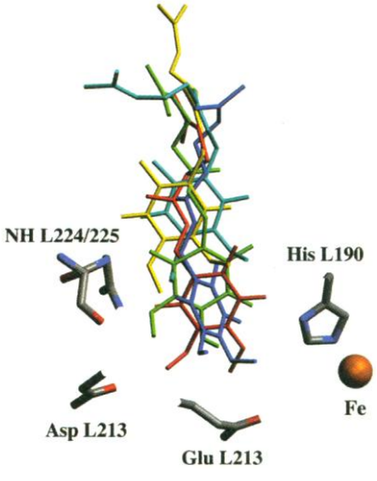

Fig. 4. Superposition of previously reported positions of ubiquinone in the Q_B binding pocket [see also (*4*)]. PDB (Protein Data Bank, Brookhaven) entries and color code: 1PCR, Ermler *et al.* (*8*), yellow; 2RCR, Chang *et al.* (*6*), dark blue; 1YST, Arnoux *et al.* (*7*), green; 4RCR, Allen *et al.* (*5*), red; present model of the dark structure, light blue. Superposition was performed by the method of Kabsch (*52*). Side chain residues from the current dark structure are indicated. Oxygen, nitrogen, and carbon atoms are colored red, blue, and gray, respectively.

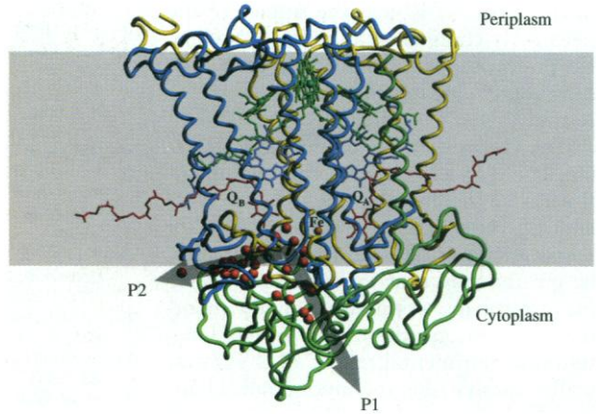

Fig. 5. Water channels P1 and P2 observed in the dark RC structure leading from the Q_B pocket to the surface of the protein on the cytoplasmic side of the RC. The coloring scheme is: H subunit (green), L subunit (yellow), M subunit (blue), water molecules (red), bacteriochlorophylls (green), and bacteriopheophytin (purple). Q_A and Q_B are colored orange-red, while the nonheme iron is rust-colored. The positions of the quinone tails past carbon C16 are less well defined because of poor electron density. The approximate location of the membrane is indicated by the shaded region. The details of the P1 and P2 pathways are shown in Fig. 6, A and B.

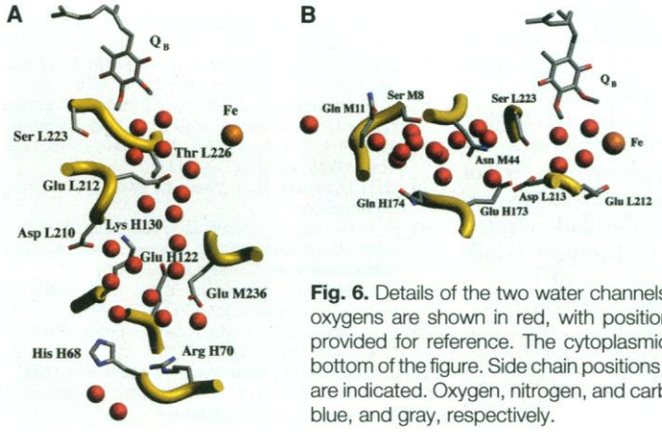

Fig. 6. Details of the two water channels P1 (**A**) and P2 (**B**). Water oxygens are shown in red, with positions of ubiquinone and iron provided for reference. The cytoplasmic side of the RC is at the bottom of the figure. Side chain positions from the dark RC structure are indicated. Oxygen, nitrogen, and carbon atoms are colored red, blue, and gray, respectively.

lished. In one of the *Rb. sphaeroides* RC structures, the positions of water molecules have been described (*8*); the locations of water molecules were also inferred by a computational approach (*39*).

The higher resolution of this work made it possible to determine the positions of a large number of water molecules, giving rise to several possible water channels (proton paths) connecting Q_B to the aqueous phase. Two of these are indicated as P1 and P2 (Fig. 5). Pathway P1 (Fig. 6A) proceeds ~23 Å from the Q_B site via Glu^{L212} through the H subunit to the cytoplasm. This pathway is approximately normal to the membrane surface and is similar to the one previously described (*8*). The second pathway, P2, which had been previously proposed (*32*) has now been identified (Fig. 6B). It leads from Ser^{L223} to Asp^{L213} via the interface between the H and M subunits, parallel to the membrane surface at approximately the depth of the nonheme iron. This pathway traverses a number of residues that have been identified by mutational studies to be involved in proton uptake by Q_B. These include Ser^{L223} (*33*), Asp^{L213} (*34, 35*), and Glu^{H173} (*36, 37*). The terminus of this pathway is near the surface of the negatively charged membrane (*40*) where the proton concentration is expected to be substantially greater than that in bulk water (*41*).

For the release of quinol and its replacement by ubiquinone, the binding affinities of the three species Q_BH_2, Q_B^-, and Q_B must meet certain criteria for proper function. The affinity for Q_B^- must be greater than that for Q_BH_2 and Q_B to prevent the loss of the functionally important Q_B^- intermediate and to avoid potentially detrimental release of the chemically reactive ubisemiquinone radical anion. The affinity of the RC for Q_B should be greater than for Q_BH_2 to thermodynamically favor the replacement of the quinol with ubiquinone. This ensures the presence of an electron acceptor for continuing ubiquinone reduction. Indeed, the observed binding affinities correspond to these expectations (*19, 30, 42*), that is, the affinities decrease in the order $Q_B^- > Q_B > Q_BH_2$. These results are readily explained by the current structures. As discussed above, both carbonyl oxygens of Q_B^- form multiple close (<2.9 Å) hydrogen bonds, whereas in the dark-adapted structure, only one of the hydrogen bonds to Q_B (NH of Ile^{L224}) is present (Figs. 2 and 3). For ubiquinol, both carbonyl oxygens are protonated, resulting in weaker binding. The release of ubiquinol may be further facilitated by the presence of the water channels.

By cooling crystals of the RC to low temperature under illumination, we have determined the structural changes around the Q_B site accompanying light-induced charge separation in bacterial RCs. These changes provide an explanation for the observed temperature dependence of the electron transfer kinetics from $Q_A^-Q_B$ to $Q_AQ_B^-$. In addition, these results account for the relative binding affinities of the different ubiquinone species in the Q_B binding pocket and identify several proton transfer pathways to the Q_B pocket that are critical for efficient function of the RC in photosynthesis.

REFERENCES AND NOTES

1. G. Feher, J. P. Allen, M. Y. Okamura, D. C. Rees, *Nature* **339**, 111 (1989).
2. R. E. Blankenship, M. T. Madigan, C. E. Bauer, Eds., *Anoxygenic Photosynthetic Bacteria* (Kluwer, Dordrecht, Netherlands, 1995).
3. J. Deisenhofer, O. Epp, K. Miki, R. Huber, H. Michel, *Nature* **318**, 618 (1985); J. Deisenhofer, O. Epp, I. Sinning, H. Michel, *J. Mol. Biol.* **246**, 429 (1995).
4. C. R. D. Lancaster and H. Michel, in *Reaction Centers of Photosynthetic Bacteria*, M. E. Michel-Beyerle, Ed. (Springer-Verlag, Berlin, 1995), pp. 23–37.
5. J. P. Allen *et al.*, *Proc. Natl. Acad. Sci. U.S.A.* **83**, 8589 (1986); J. P. Allen, G. Feher, T. O. Yeates, H. Komiya, D. C. Rees, *ibid.* **84**, 5730 (1987); *ibid.* **85**, 8487 (1988).
6. C. H. Chang *et al.*, *FEBS Lett.* **205**, 82 (1986); O. E. Kabbani, C. H. Chang, J. Tiede, J. Norris, M. Schiffer, *Biochemistry* **30**, 5352 (1986).
7. B. Arnoux, J. F. Gaucher, A. Ducruix, F. Reiss-Husson, *Acta Crystallogr. D* **51**, 368 (1995).
8. U. Ermler, G. Fritzsch, S. Buchanan, H. Michel, in *Research in Photosynthesis*, N. Murata, Ed. (Kluwer, Amsterdam, 1992), pp. 341–347; U. Ermler, G. Fritzsch, S. K. Buchanan, H. Michel, *Structure* **2**, 925 (1994).
9. P. P. Noks, E. P. Lukashev, A. A. Komonekko, P. S. Benedikto, A. B. Rubin, *Mol. Biol. (Moscow)* **11**, 1090 (1977).
10. H. Arata and W. W. Parson, *Biochim. Biophys. Acta* **636**, 70 (1981); *ibid.* **638**, 201 (1981).
11. D. Kleinfeld, M. Y. Okamura, G. Feher, *Biochemistry* **23**, 5780 (1984).
12. N. W. Woodbury and W. W. Parson, *Biochim. Biophys. Acta* **767**, 345 (1984).
13. C. Kirmaier, D. Holten, W. W. Parson, *ibid.* **810**, 33 (1985).
14. P. Parot, J. Thiery, A. Vermeglio, in *The Photosynthetic Bacterial Reaction Center*, J. Breton and A. Vermeglio, Eds. (Plenum, New York, 1988), pp. 251–260.
15. E. Nabedryk *et al.*, *FEBS Lett.* **266**, 59 (1990).
16. J. P. Allen, *Proteins* **20**, 283 (1994).
17. J. A. Isaacson, F. Lendzian, E. C. Abresch, W. Lubitz, G. Feher, *Biophys. J.* **69**, 311 (1995).
18. M. Y. Okamura, R. J. Debus, D. Kleinfeld, G. Feher, in *Function of Quinones in Energy Conserving Systems*, B. L. Trumpower, Ed., (Academic Press, New York, 1982), vol. 5, pp. 99–117.
19. M. H. B. Stowell, G. Y. Wang, M. W. Day, S. I. Chan, in preparation.
20. H. Hope, *Stanford Synchrotron Radiation Laboratory 22nd Annual Users Meeting, Workshop on Techniques in Macromolecular Crystallography* (1995).
21. H. D. Bellamy, R. P. Phizackerley, S. M. Soltis, H. Hope, *J. Appl. Crystallogr.* **27**, 967 (1994).
22. J. D. McElroy, D. C. Mauzecall, G. Feher, *Biochim. Biophys. Acta* **333**, 261 (1974).
23. J. Breton and E. Nabedryk, *ibid.* **1275**, 84 (1996).
24. I. Sinning, H. Michel, P. Mathis, A. W. Rutherford, *Biochemistry* **28**, 5544 (1989).
25. M. Y. Okamura, R. A. Isaacson, G. Feher, *Proc. Natl. Acad. Sci. U.S.A.* **72**, 3491 (1975); C. A. Wraight and R. R. Stein, in *The Oxygen Evolving System of Photosynthesis*, Y. Inoue *et al.*, Eds. (Academic Press, London and New York, 1983), vol. 2, pp. 383–392.
26. M. L. Paddock, E. Abresch, R. A. Isaacson, G. Feher, M. Y. Okamura, *Biophys. J.* **72** (abstr. A8) (1997).
27. D. Kleinfeld, M. Y. Okamura, G. Feher, *Biochim. Biophys. Acta* **766**, 126 (1984); L. J. Mancino, D. P. Dean, R. E. Blankenship, *ibid.* **764**, 46 (1984).
28. M. S. Graige, G. Feher, M. Y. Okamura, *Biophys. J.* **70**, Abstr A10 (1996).
29. P. Brzezinski, M. Y. Okamura, G. Feher, in *The Photosynthetic Bacterial Reaction Center II*, J. Breton and A. Vermeglio, Eds. (Plenum, New York, 1992), pp. 321–330.
30. P. H. McPherson, M. Y. Okamura, G. Feher, *Biochim. Biophys. Acta* **1016**, 289 (1990).
31. W. A. Cramer and D. B. Knaff, *Energy Transduction in Biological Membranes* (Springer-Verlag, New York, 1990).
32. M. Y. Okamura, G. Feher, *Ann. Rev. Biochem.* **61**, 861 (1992).
33. M. L. Paddock, P. H. McPherson, G. Feher, M. Y. Okamura, *Proc. Natl. Acad. Sci. U.S.A.* **87**, 6803 (1990).
34. E. Takahashi and C. A. Wraight, *Biochim. Biophys. Acta* **1020**, 107 (1990).
35. M. L. Paddock *et al.*, *Biochemistry* **33**, 734 (1994).
36. S. H. Rongey, A. L. Juth, M. L. Paddock, G. Feher, M. Y. Okamura, *Biophys. J.* **68**, A247 (1995).
37. E. Takahashi and C. A. Wraight, *Proc. Natl. Acad. Sci. U.S.A.* **93**, 2640 (1996).
38. S. H. Rongey, M. L. Paddock, G. Feher, M. Y. Okamura, *ibid.* **90**, 1325 (1993).
39. P. Beroza, D. R. Fredkin, M. Y. Okamura, G. Feher, in *The Photosynthetic Bacterial Reaction Center II*, J. Breton and A. Vermeglio, Eds. (Plenum, New York, 1992), pp. 363–374.
40. J. Barber, *Biochim. Biophys. Acta* **594**, 253 (1980).
41. S. McLaughlin, *Curr. Top. Membr. Transport* **9**, 71 (1977); A. P. Winiski, A. C. McLaughlin, R. V. McDaniel, M. Eisenberg, S. McLaughlin, *Biochemistry* **23**, 8206 (1986); S. C. Hartsel and D. S. Cafiso, *ibid.* **25**, 8214 (1986).
42. C. A. Wraight, *Isr. J. Chem.* **21**, 348 (1981); B. A. Diner, C. C. Schenck, C. DeVitry, *Biochim. Biophys. Acta* **776**, 9 (1984).
43. Z. Otwinowski, in *Data Collection and Processing*, L. Sawyer, L. Isaacs, S. Bailey, Eds., (SERC Daresbury Laboratory, Daresbury, UK, 1993), pp. 56–62.
44. S. Bailey, *Acta Crystallogr.* **D50**, 760 (1994).
45. P. M. D. Fitzgerald, *J. Appl. Crystallogr.* **21**, 273 (1988).
46. W. A. Hendrickson and E. E. Lattman, *Acta Crystallogr.* **B26**, 136 (1970).
47. W. Furey and S. Swaminathan, *Am. Crypt. Assoc. Mtg. Abstr. Ser. 2* **18**, 73 (1990).
48. J. P. Abrahams and A. Leslie, *Acta Crystallogr.* **D52**, 30 (1996).
49. T. A. Jones, *Methods Enzymol.* **115**, 157 (1985); T. A. Jones, J. Y. Zhou, S. W. Cowan, M. Kjeldgaard, *Acta Crystallogr.* **A47**, 110 (1991).
50. A. T. Brünger, J. Kuriyan, M. Karplus, *Science* **235**, 458 (1987).
51. S. V. Evans, *J. Mol. Graphics* **11**, 134 (1993).
52. W. Kabsch, *Acta Crystallogr.* **A32**, 922 (1976).

53. We thank M. Y. Okamura, M. L. Paddock, H. L. Axelrod, and M. S. Graige for insightful comments and discussions. This work was supported by grants from the National Institutes of Health (NIH GM13191, NIH GM45162). The rotation camera facility at SSRL is supported by the Department of Energy and by NIH. X-PLOR calculations were performed at the San Diego Supercomputer Center supported by NSF. The coordinates have been deposited in the Brookhaven Protein Data Bank with accession number 1aig and aij.

18 September 1996; accepted 10 March 1997